Fluctuation-induced current from freestanding graphene

P. M. Thibado [1,*] P. Kumar,[1] Surendra Singh,[1] M. Ruiz-Garcia,[2] A. Lasanta,[3,4] and L. L. Bonilla[3,5,†]

[1]*Department of Physics, University of Arkansas, Fayetteville, Arkansas 72701, USA*

[2]*Department of Physics, University of Pennsylvania, Philadelphia, Pennsylvania 19104, USA*

[3]*G. Millán Institute for Fluid Dynamics, Nanoscience and Industrial Mathematics and Department of Mathematics,*
Universidad Carlos III de Madrid, 28911 Leganés, Spain

[4]*Departamento de Álgebra, Facultad de Educación, Economía y Tecnología de Ceuta, Universidad de Granada, E-51001 Ceuta, Spain*

[5]*Courant Institute for Mathematical Sciences, New York University, New York, New York 10012, USA*

At room temperature, micron-sized sheets of freestanding graphene are in constant motion, even in the presence of an applied bias voltage. We quantify the out-of-plane movement by collecting the displacement current using a nearby small-area metal electrode and present an Ito-Langevin model for the motion coupled to a circuit containing diodes. Numerical simulations show that the system reaches thermal equilibrium and the average rates of heat and work provided by stochastic thermodynamics tend quickly to zero. However, there is power dissipated by the load resistor, and its time average is exactly equal to the power supplied by the thermal bath. The exact power formula is similar to Nyquist's noise power formula, except that the rate of change of diode resistance significantly boosts the output power, and the movement of the graphene shifts the power spectrum to lower frequencies. We have calculated the equilibrium average of the power by asymptotic and numerical methods. Excellent agreement is found between experiment and theory.

I. INTRODUCTION

Freestanding, two-dimensional (2D) crystalline membranes exhibit unique out-of-plane motion [1,2]. When relaxed, sheets of freestanding graphene feature a rippled morphology, in which adjacent regions alternate between concave and convex curvature [3]. The origin of these nanometer-sized ripples is still an open question [4,5]. Theoretical work points to electron-phonon coupling as the source because it suppresses long-wavelength bending rigidity and enhances off-plane fluctuations [6–8]. In a state of thermal equilibrium, Guinea *et al.* derived a system of equations for the height of a graphene membrane including auxiliary stress and curvature fields [8]. Within this perturbative formulation of quantum statistical mechanics, circular graphene membranes spontaneously buckle below a critical temperature and above a critical radius [9]. Numerical studies of static rippling in a membrane coupled with Dirac fermions show a phase transition from flat to rippled morphology [10].

Early phenomenological studies of dynamic fluctuations modeled the electron-phonon interaction by coupling point particles at the nodes of a hexagonal lattice to Ising spins that undergo Glauber dynamics [11,12]. The spins exchange energy with a thermal bath, their dynamics show rippling, and their interaction with the membrane drives the whole system to equilibrium [13].

A. Flexible and inflexible freestanding graphene

The first reported experimental studies of freestanding graphene using scanning tunneling microscopy (STM) were published in 2012 [14–18]. Due to the slow scanning nature of STM, images of the moving graphene were too noisy to be meaningful. Sample quality and cleanliness became the primary focus in the drive to develop methods to stabilize the surface. It was then discovered that after applying voltage ramps with the feedback on, the graphene was quickly pulled and became inflexible, making it possible to obtain atomic resolution STM images [19–24]. The surfaces were clean and the honeycomb pattern evident. This new technique led to research on two types of freestanding graphene: flexible and inflexible. Studies on *flexible* graphene could then move forward, shifting from imaging mode to point-mode. In point-mode, the STM acquires data at much higher rates, continuously tracking the random up and down movements of the graphene. Time-series data appear similar to one-dimensional random walks. This is consistent with electron mobility measurements that indirectly confirm the presence of thermal vibrations [25]. This novel use of STM allows a rich set of stochastic tools normally used in soft-matter physics to be applied to inorganic crystals [26].

Experiments by Ackerman *et al.* measured the out-of-plane motion of atoms in freestanding graphene using point-mode STM [2]. They show that single atoms in the membrane experience Brownian motion with sporadic large jumps that are typical of Lévy processes [2,27]. Rare jumps in the height of the graphene atoms correspond to coherent inversions of the curvature of the ripples on which the atoms sit. This understanding is rigorously supported by both molecular dynamics [2] and spin-membrane Glauber dynamics [13,28].

*Corresponding author: thibado@uark.edu

†Corresponding author: bonilla@ing.uc3m.es

B. Theory and experiments of fluctuating freestanding graphene

We have studied the thermal fluctuations of freestanding graphene membranes using point-mode STM. To minimize the influence of the STM feedback circuit on fluctuations, we disabled it in a controlled manner and backed the tip away from the surface. With the feedback disabled, we operated the STM in constant-height mode rather than constant-current mode. This allows us to measure the displacement current resulting from graphene moving relative to the tip. While constant-height mode precludes mapping the surface of graphene and directly measuring the distance to the STM tip, we can measure the fluctuating current and dissipated power. The average dissipated power is very small for the bias voltage up to about 10 V but increases noticeably beyond that. Our observations allow us to introduce a model of freestanding graphene coupled to an electric circuit. Spontaneous thermal fluctuations in a soft and flexible freestanding graphene membrane are envisioned as random flipping of the ripple closest to the STM tip between convex and concave shapes. The ripple acts as a Brownian particle in a double-well potential subject to friction, thermal noise, and the interaction with STM tip and circuit. To this end, ripple and STM tip act as a capacitor of variable capacitance, which is inversely proportional to the distance between ripple and tip. The electrical circuit includes two diodes in parallel and opposition, which act as nonlinear resistors and enable measurement of displacement current flowing counter to the bias voltage. Resistor noise implies that we need to include both state dependent Nyquist noise and a temperature-dependent drift term in the circuit equations. We have studied the stochastic thermodynamics of the resulting novel equations. When the graphene moves away from the tip, charge must flow counter to the bias voltage and perform electrical work. We calculated the equilibrium average of the power dissipated at the diodes, both numerically and by asymptotic methods, and fit it to the experimental results. This calculation shows that the power varies many orders of magnitude for realistic values of the parameters. We have also simulated the stochastic equations using convenient parameter values that make possible their numerical integration. These simulations show that long-time averages combined with ensemble averages agree with equilibrium averages. Our model provides a rigorous demonstration that continuous thermal power can be supplied by a Brownian particle at a single temperature while in thermodynamic equilibrium, provided the *same amount* of power is continuously dissipated in a resistor. Here, coupling to the circuit allows electrical work to be carried out on the load resistor without violating the second law of thermodynamics.

The paper is structured as follows. The STM experiments and results are described in Sec. II. The theoretical model is introduced in Sec. III, in which we derive the Ito-Langevin equations for graphene ripple, STM tip, and electrical circuit containing diodes as nonlinear resistors. These equations can also be derived from a master equation formulation for elementary charges arriving at the plates of the graphene-STM tip variable capacitor, as explained in Appendix A. Section IV is devoted to the modeling of stochastic thermodynamics. We derive formulas for the heat flux produced by friction and random forces acting on the graphene ripple and for work

flux created by the circuit on the ripple. We calculate the equilibrium average of the power dissipated at the diodes, which is found to be different from zero but equal to the average power provided by the thermal bath. Some technical details are relegated to Appendix B. We compare theory and experiments in Sec. V. Section VI contains a discussion and summary of our results.

II. STM EXPERIMENTS AND RESULTS

For this study, graphene was commercially grown on Ni and then dry transferred to a 2000-mesh, ultrafine copper grid featuring a lattice of square holes (each 7.5 μm wide) and bar supports (each 5 μm wide). The graphene sample is larger than the transmission electron microscope (TEM) grid and covers it entirely. Excess graphene bonds to the side wall [29]. We have previously published scanning electron microscope images and confirmed 90% coverage of the grid [17]. We have also previously published numerous atomic resolution STM images of graphene on the copper bar supports of the TEM grid and of freestanding graphene after being pulled to an inflexible state using voltage ramps [17,21].

An Omicron ultrahigh vacuum STM (base pressure 10^{-10} mbar) operated at room temperature was used. From our experience, if the graphene film is mounted toward the STM tip, then it can be pulled off the copper grid. Therefore, for this study the graphene film was mounted toward the sample plate on standoffs, forcing the STM tip to approach the graphene through the grid holes. The entire STM chamber rests on an active, noise-cancelling, vibration isolation system and is powered using a battery bank with an isolated ground to suppress mechanical and electrical noise.

A. STM tunneling

The STM tip-sample junction is incorporated into the circuit as shown in Fig. 1(a). The sample is isolated from ground and connected to two diodes. This is a custom modification to our STM as well as a new use for STM [30]. In our circuit, the tip-sample junction acts as a variable capacitor [31–34]. The tunneling current, diode 1 current (D1C), and diode 2 current (D2C) are monitored simultaneously. This diode arrangement is normally used for energy harvesting, but here we use it to isolate the displacement current from the tunneling current. *For positive bias voltages the tunneling current cannot flow through D2.* The smallest current we measure is 1 pA. At a tip-sample distance of 2 nm or less, the tunneling current dominates ($\geqslant$100 pA) and flows through D1; for larger distances and higher bias voltages, the displacement current dominates ($\geqslant$100 pA) and which flows through D2.

An illustration of rippled graphene and voltage-induced shape changes is shown in Fig. 1(b). When the bias voltage increases, the graphene is stretched and the STM tip moves with the graphene. We attribute this movement to the applied electric force, which was characterized in our earlier studies on the effect of voltage ramps [35]. A typical constant-current point-mode STM measurement of the membrane height in time is shown in Fig. 1(c). During this experiment, the STM tip only moves vertically. Note the enormous size of the movement, as compared to atomic corrugations of less than 0.1 nm.
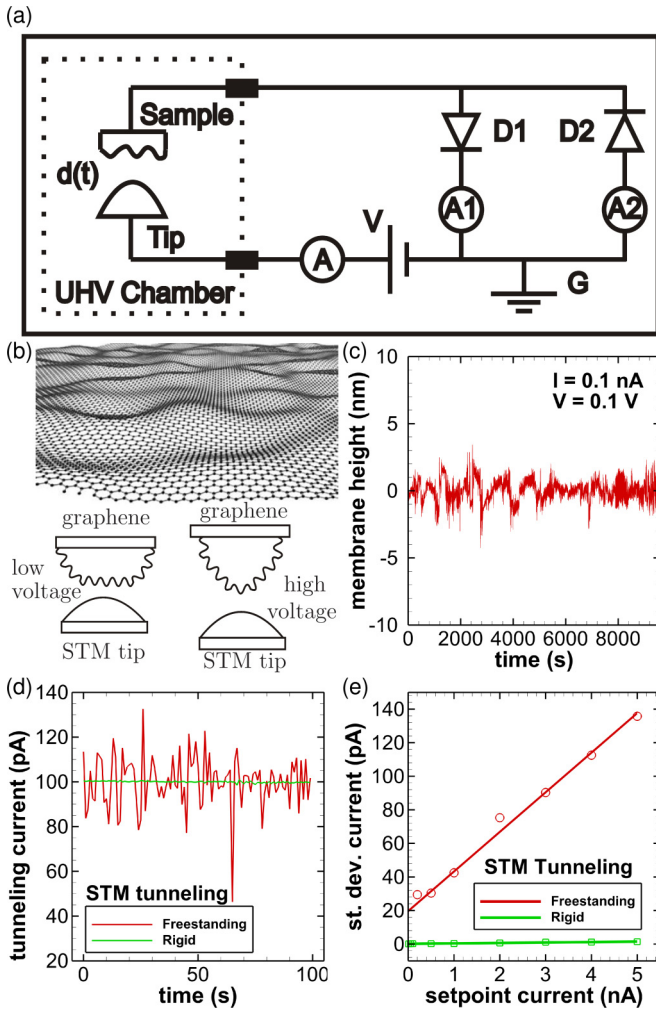
FIG. 1. STM data sets acquired when STM tip is tunneling electrons. (a) Circuit diagram showing STM tip, sample, bias voltage, ammeters, and diode arrangement. (b) Sketch of graphene sheet in rippled state and illustrations of graphene shape changes. (c) Height fluctuations of graphene. (d) STM tunneling current vs. time for freestanding and rigid graphene. (e) Standard deviation of tunneling current vs. setpoint current for freestanding and rigid graphene.

We have previously published similar data sets, and these data show that it is possible to maintain stable tunneling for hours and continuously track graphene's movement. This is one of the key benefits of point mode. The tunneling current in time is shown in Fig. 1(d) for both rigid graphene (i.e., graphene on copper) and flexible freestanding graphene. For the freestanding sample, the average current is the same as the rigid sample, but the fluctuations are 100 times larger (10 pA vs. 0.1 pA). The result shown in Fig. 1(d) is independent of the applied bias voltage (up to 3 V) and feedback gain setting. As the setpoint current (SPC) increases, the standard deviation also increases, as shown in Fig. 1(e). We attribute this to sample heating. This was previously studied in an effort to separate tunneling current effects from bias voltage effects [35]. When extrapolated to zero tunneling current, the fluctuations still contribute 20 pA of current. Here the freestanding graphene data are taken from *flexible* graphene that is suspended over the copper TEM grid holes. When this type of measurement
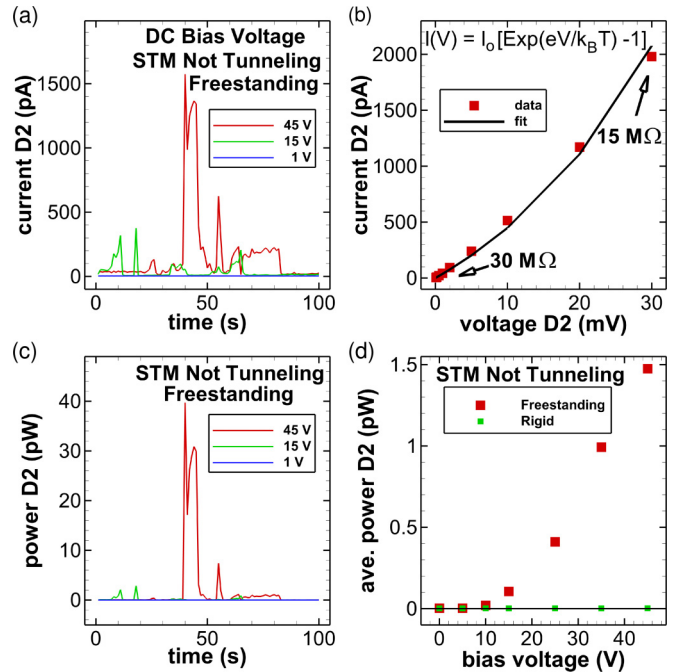

FIG. 2. STM data sets acquired when the STM tip is not tunneling electrons. (a) Current through diode 2 versus time for voltages $V = 1, 15, 45$ V. (b) Average current vs. voltage through diode 2. (c) Power through diode 2 vs. time for different voltages. (d) Average power through diode 2 vs. voltage bias V.

is repeated for rigid graphene, we see no noticable variation in the standard deviation with SPC, as shown in the lower half of Fig. 1(e). These are data taken from graphene supported by copper. We often tunnel directly to the copper bar supports, as well, which also shows a constant tunneling current with the same small standard deviation. This is the noise level of our electronics.

B. STM displacement current

To measure the displacement current at zero tunneling current, we incrementally backed the STM tip away from the sample using the coarse motion stage until the distance was too great for electrons to tunnel through the vacuum barrier. The coarse motion stage uses a stick-slip mechanism that provides irregular jumps of about 10 nm. The tip tends to move farther when moving away from the sample (down with gravity) compared to moving toward the sample (up against gravity). It does not require a lot of time, but the tip is moved back and forth until the right conditions are met. In this position, the SPC is set to 50 nA, thereby using the feedback circuit to keep the STM tip stationary (i.e., fully forward). We then increase the dc bias voltage and monitor the diode currents. The criteria for having found the proper tip positon is to allow no constant tunneling current in D1 and to maintain a pulsing current in D2. Typical displacement currents flowing through D2 in time are shown in Fig. 2(a). At 1 V, no current is induced, but at 15 V and 45 V, we consistently observed a spiky, time-dependent D2C. If a tunneling current was detected in D1, then we would stop taking data and reposition the tip farther from the graphene. This
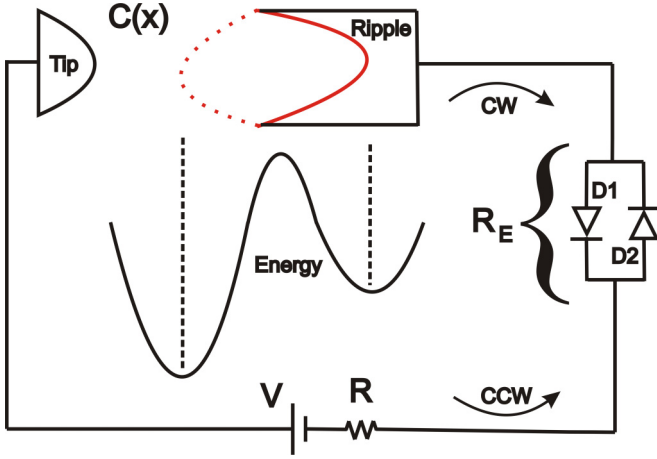
FIG. 3. Sketch of circuit model with energy barrier diagram.

is done either by taking coarse motion steps away from the graphene or by fine adjustment of the lateral position of the tube scanner.

We have studied the displacement current at various locations across the freestanding graphene and observe a trend. For locations near the center of the freestanding graphene sheet, the movement of the graphene can sometimes be too large and too rapid to even maintain tunneling. Under these conditions, we would move to a new location. For locations near the copper support bar, we cannot observe a displacement current in D2. The STM is either tunneling or we do not see any current. The data collected are similar to that presented in green in Fig. 1(e) for rigid surface tunneling.

The low current I-V characteristics of D2 were also measured and are shown in Fig. 2(b) with resistance labels. Combining this voltage data with the displacement current data in Fig. 2(a), the power dissipated in D2 was calculated and is shown in Fig. 2(c). The maximum instantaneous power reached is 40 pW. The average power for a large number of data sets acquired across this sample and other identically prepared samples of flexible freestanding graphene is shown in Fig. 2(d). The average power significantly rises for bias voltages above 10 V. When this same measurement is repeated for rigid graphene, we do not observe a D2C. This result is shown near the bottom of Fig. 2(d). Of course, the D2C flows opposite the bias voltage. Only a displacement current can flow in this direction. Any current due to field emmision effects, for example, will flow through D1.

III. GRAPHENE AND CIRCUIT MODEL

A. Graphene membrane and STM tip

The power dissipated in D2 suggests that electrical work is done on D2 by the motion of the graphene even though it is held at a single temperature (i.e., room temperature). Of course, Nyquist showed that one resistor can perform work on another resistor at a single temperature while in thermodynamic equilibrium, provided the *same amount* of work is done in return [36]. A deeper understanding of this phenomenon will shed light on our more complex system. To this end, we developed the model shown in Fig. 3.

The carbon atom closest to the STM tip sits over a ripple, which fluctuates between convex and concave curvature. We model the membrane atoms closer to the tip as a Brownian particle in a double-well potential, which represents the convex and concave curvature states of the ripple [2]. The particle is in contact with a thermal bath at temperature T (in units of energy). The Ito-Langevin equation of motion for the particle including the damping force $-\eta v$ and a thermal noise satisfying the Einstein relation take the form:

$$dx = v\, dt, \tag{1a}$$

$$m\, dv = \left[-\eta v - U'(x) - \frac{q^2 - C_0(V)^2 V^2}{2C_0(V)d} \right] dt$$

$$+ \sqrt{2T\eta}\, dw_p, \tag{1b}$$

$$U(x) = U_B \left(\frac{x^4}{4l^4} - \frac{x^2}{2l^2} \right), \tag{1c}$$

$$C(x) = \frac{C_0(V)}{1 + \frac{x}{d}}, \quad C_0(V) = \frac{\varepsilon A(V)}{d} = C_0\, \Gamma(V). \tag{1d}$$

Here $w_p(t)$ is a zero mean Wiener noise. The STM tip and sample act as a variable capacitor, $d + x(t)$ and $x(t)$ ($x \ll d$) are, respectively, the instantaneous distances between STM tip and sample and the vertical position of the Brownian particle measured with respect to the flat configuration of the graphene membrane. In the double-well potential $U(x)$, U_B and l measure the barrier height and the ripple size, respectively. If the instantaneous charge and voltage drop of the tip-sample capacitor are $q(t)$ and $u(t)$, respectively, then the electrostatic force exerted on the particle is $qu/[2(d + x)] = q^2/[2C_0(V)d]$, where $u = q/C(x)$. In addition, the graphene sheet is deformed so that the region immediately under the tip sharpens; as illustrated in Fig. 1(b). The area of this region then decreases from the value $A(0)$, which is indicated by the decreasing function $\Gamma(V)$ in Eq. (1d). To compensate for the oversimplification of substituting a mass particle instead of a ripple in a membrane, we add a constant tension $\frac{C_0 V^2}{2d}$ to Eq. (1b) due to stretching of graphene. Then by defining the Hamiltonian function as

$$\mathcal{H}(x, p, q) = \frac{p^2}{2m} + U(x) + \frac{q^2}{2C(x)} - \frac{C_0(V)V^2 x}{2d} + qV, \tag{2}$$

Eq. (1) can be written as

$$dx = \frac{\partial \mathcal{H}}{\partial p}\, dt = \frac{p}{m}\, dt, \tag{3a}$$

$$dp = -\left(\frac{\eta}{m} p + \frac{\partial \mathcal{H}}{\partial x} \right) dt + \sqrt{2T\eta}\, dw_p. \tag{3b}$$

B. Circuit equation

The Ito-Langevin equation for charge q through the equivalent resistor (diodes of resistances R_j and linear resistor R) is as follows:

$$dq = \left[\frac{\partial}{\partial q} \left(\frac{T}{\mathcal{R}} \right) - \frac{1}{\mathcal{R}} \frac{\partial \mathcal{H}}{\partial q} \right] dt + \sqrt{\frac{2T}{\mathcal{R}}}\, dw_q, \tag{4a}$$

$$\frac{\partial \mathcal{H}}{\partial q} = V + \frac{q}{C(x)}, \tag{4b}$$

where w_q is a Wiener noise independent of w_p and equivalent resistance $\mathcal{R} = R + R_E$ with $R_E^{-1} = R_1^{-1} + R_2^{-1}$. Equation (4b) provides the voltage drop $V_{\mathcal{R}}(x) = V + q/C(x)$ across the equivalent resistor $\mathcal{R}$. For identical ideal diodes having $I_1(u_D) = i_D(u_D) = I_0(e^{u_D/T_e} - 1)$ and $I_2 = i_D(-u_D)$, the equivalent resistance is $R_E^{-1} = \frac{2I_0}{u_D} \sinh \frac{u_D}{T_e}$, where u_D is the voltage drop across the diodes, I_0 the saturation current, and $T_e = \frac{T}{e}$. Equation (4a) is derived here for the first time. Next, we show how we arrived at the first term in Eq. (4a).

For a constant resistance $\mathcal{R}$, the first term in Eq. (4a) is zero and the resulting equation contains the usual Nyquist noise associated with a resistor $\mathcal{R}$ at temperature T. Then the Fokker-Planck equation (FPE) corresponding to Eqs. (3) and (4) is

$$
\frac{\partial \rho}{\partial t} = -\frac{\partial}{\partial x}\left(\frac{\partial \mathcal{H}}{\partial p}\rho\right) + \frac{\partial}{\partial p}\left[\frac{\partial \mathcal{H}}{\partial x}\rho + \eta\left(\frac{p}{m}\rho + T\frac{\partial \rho}{\partial p}\right)\right]
$$
$$
+ \frac{\partial}{\partial q}\left[\frac{1}{\mathcal{R}}\left(\frac{\partial \mathcal{H}}{\partial q}\rho + T\frac{\partial \rho}{\partial q}\right)\right]. \quad (5)
$$

The stationary solution of Eq. (5) is the equilibrium probability density proportional to $e^{-\mathcal{H}/T}$. It is globally and asymptotically stable, as any initial probability density will evolve to it [37]. For a nonlinear resistor, $\mathcal{R}(u)$ is a function of the overall charge q. Using Kirchhoff's laws, we derive in Appendix A the following relation between u and q:

$$
u\left(1 + \frac{R}{R_E(u)}\right) = u + 2I_0 R \sinh\left(\frac{u}{T_e}\right) = V + \frac{q}{C}. \quad (6)
$$

If we postulate that Eq. (5) is correct for a nonconstant resistance $\mathcal{R}(u_D)$, then

$$
\frac{\partial}{\partial q}\left(\frac{T}{\mathcal{R}}\frac{\partial \rho}{\partial q}\right) = T\frac{\partial^2}{\partial q^2}\left(\frac{1}{\mathcal{R}}\rho\right) - \rho\frac{\partial}{\partial q}\left(\frac{T}{\mathcal{R}}\right). \quad (6')
$$

The last term yields the correction to the drift term that appears in the Ito-Langevin equation (4). The FPE (5) can also be obtained from a master equation as described in Appendix A.

IV. STOCHASTIC THERMODYNAMICS

A. Average generated power

From the point of view of the graphene ripple, represented by the particle in Eq. (1), the circuit is an external system that does work on it. The heat produced by friction and noise forces is then [26]

$$
d'Q = \left(-\eta\frac{p}{m} + \sqrt{2T\eta}\frac{dw_p}{dt}\right) \circ dx(t)
$$
$$
= d\mathcal{H}(x, p, q) - \frac{\partial \mathcal{H}}{\partial q} \circ dq(t), \quad (7)
$$

in which the charge $q = q(t)$ acts as an external parameter and we have used Eqs. (2) and (3). Here $d'Q > 0$ if heat is absorbed by the particle, and the product $\circ$ with differentials is taken in the Stratonovich sense. Here d' indicates a small amount of the quantity; not a differential. The Stratonovich product on the first line of Eq. (7) can be converted into an Ito

product:

$$
\frac{dw_p}{dt} \circ dx = \frac{p}{m} \circ dw_p = \frac{p}{m}dw_p + \frac{1}{2m}dp\,dw_p
$$
$$
= \frac{p}{m}dw_p + \frac{1}{2m}\sqrt{2T\eta}\,dt,
$$

in which we have used $(dw_p)^2 = dt$. Then

$$
d'Q = \frac{\eta}{m^2}(mT - p^2)dt + \sqrt{2T\eta}\frac{p}{m}dw_p(t). \quad (8)
$$

The average of the noise term in Eq. (8) vanishes due to the nonanticipative character of the Ito product, thereby yielding

$$
\left\langle\frac{d'Q}{dt}\right\rangle = \frac{\eta}{m}\left(T - \left\langle\frac{p^2}{m}\right\rangle\right). \quad (9)
$$

This average heat flux vanishes in equilibrium because of the equipartition theorem.

From the second line in Eq. (7), we obtain the first law of thermodynamics,

$$
d\mathcal{H}(x, v, q) = d'Q + d'W. \quad (10)
$$

Here the work done on the particle by the circuit is

$$
d'W = \frac{\partial \mathcal{H}}{\partial q}(x, p, q)\circ dq
$$
$$
= \frac{\partial \mathcal{H}}{\partial q}\left[\frac{\partial}{\partial q}\left(\frac{T}{\mathcal{R}}\right) - \frac{1}{\mathcal{R}}\frac{\partial \mathcal{H}}{\partial q}\right]dt + \sqrt{\frac{2T}{\mathcal{R}}}\frac{\partial \mathcal{H}}{\partial q}\circ dw_q
$$
$$
= \left[\frac{\partial}{\partial q}\left(\frac{T}{\mathcal{R}}\frac{\partial \mathcal{H}}{\partial q}\right) - \frac{1}{\mathcal{R}}\left(\frac{\partial \mathcal{H}}{\partial q}\right)^2\right]dt + \sqrt{\frac{2T}{\mathcal{R}}}\frac{\partial \mathcal{H}}{\partial q}dw_q.
$$
$$(11)$$

We have converted the Stratonovich product to an Ito product on the last line of this expression. From Eq. (11), the average power absorbed by the particle is

$$
\left\langle\frac{d'W}{dt}\right\rangle = \left\langle\frac{\partial}{\partial q}\left(\frac{T}{\mathcal{R}}\frac{\partial \mathcal{H}}{\partial q}\right)\right\rangle - \left\langle\frac{1}{\mathcal{R}}\left(\frac{\partial \mathcal{H}}{\partial q}\right)^2\right\rangle. \quad (12)
$$

Using the equilibrium probability density to calculate the average and integrating by parts, the average power absorbed by the particle is found to be zero. Since $\frac{\partial \mathcal{H}}{\partial q} = V + q/C(x) = V_{\mathcal{R}}(x)$ is the voltage drop across the equivalent resistor $\mathcal{R}$, the time-averaged power dissipated in the resistor equals the time-averaged power supplied by the thermal bath. Thus, from the resistor's perspective, the movement of the graphene ripple represents a source of power equal to the average thermal power. If $\mathcal{R}$ is held constant, then the first term in Eq. (12) is Nyquist's noise power formula $\frac{T}{\mathcal{R}C}$, while the second term $\frac{V_{\mathcal{R}}^2}{\mathcal{R}}$ is the power dissipated in the resistor. The exact result, when diodes are considered, is shown in Fig. 4.

The Nyquist result (dashed line) can be understood as follows: For low diode voltages, the diode resistance is much larger than the series resistor, so the power dissipated is low. As the diode voltage rises, its resistance drops, increasing the dissipated power. Eventually, the diode resistance is much smaller than the series resistor and the power saturates. The exact result follows a similar trend, except that it has a large power enhancement over the Nyquist result. The increase in
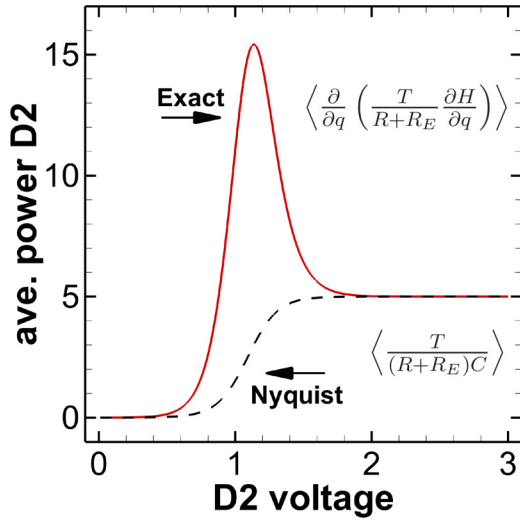
FIG. 4. Noise power vs. diode voltage showing the power enhancement over Nyquist's formula.

power, in the middle section, comes from the rate of change in resistance (with voltage across the diode) of the diode.

B. Model simulation and results

We confirmed these predictions by performing numerical simulations of the stochastic model equations (3) and (4) using the first-order Milstein numerical scheme [38]. We have chosen parameters that allow the simulation to capture the important physics in a qualitative manner. A quantitative comparison is made later. Simulations allow us to confirm that time averages of the power dissipated at the diodes are equal to time averages of power generated by thermal fluctuations. We have used the following parameters in the numerical simulations $m = 1$, $l = 1$, $U_B = 4$, $R = 0.1$, $T = 0.5$, $\eta = 1$, $d = 10$, $I_0 = 0.0002$, and $T_e = 0.1$ (see Fig. 6 panels for other parameters and alterations). To account for the graphene shape change, we have C_0 fall from 5 to 1 as V increases from 1 to 10, which is within the range of the battery voltage in our numerical simulations. To ensure numerical convergence, simulations were averaged over 10 million time steps and 1 million realizations. The long time interval used to calculate time averages ensures that thermal equilibrium is reached and time averages equal equilibrium averages. As another check, we also ran separate simulations using either Stratonovich or Ito protocols and confirmed the averages agreed with one another.

The particle's position randomly moves between the two minima of the double-well potential, as shown in Fig. 5(a). This position plus d is the distance to the tip. So, as the particle moves, the capacitance, C, of the circuit is modified. The overall charge on the capacitor fluctuates in time about the average value, $-CV$, and has multiplicative noise, as shown in Fig. 5(b). As the charge changes, the electric force on the particle is modified. These interactions provide the intimate coupling that ultimately works to maintain thermodynamic equilibrium with each time step. The current flowing through the circuit is shown in Fig. 5(c), and the power dissipated in D2 is shown in Fig. 5(d).
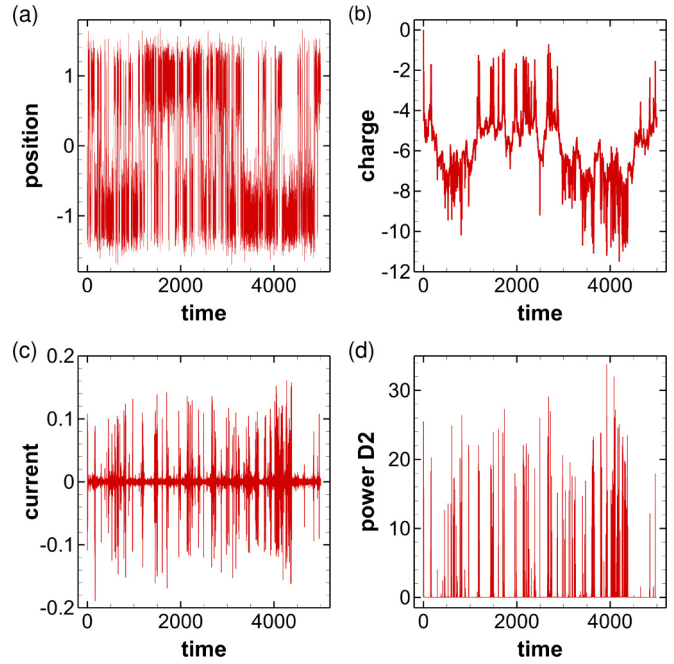

FIG. 5. Ito-Langevin equation simulation results for a circuit with diodes and resistor. (a) Height of graphene ripple x, (b) charge q, (c) total current, and (d) power dissipated in D2 versus time.

For this study, we are interested in the direction of current flow, either clockwise through D1 or counterclockwise through D2. Using the value of $\dot{q}$, we have separately calculated the average power generated and dissipated from the dynamics, using Eq. (12) for each half cycle. Even in the half cycle, the two power terms are equal. The average power (both generated and dissipated), along with Nyquist's prediction, is shown in Fig. 6(a). The power is found to increase with bias voltage, which is qualitatively similar to our experimental results. This result is unusual given that the power dissipated in a resistor is independent of bias voltage, according to Nyquist $\frac{V_{\mathcal{R}}^2}{\mathcal{R}} = \frac{T}{\mathcal{R}C}$. However, for flexible graphene, the capacitance decreases as the bias voltage increases. As a result, the voltage drop across the resistor increases, $V_{\mathcal{R}}^2 = \frac{T}{C}$. For the case with diodes, as the voltage increases, the diode resistance drops.
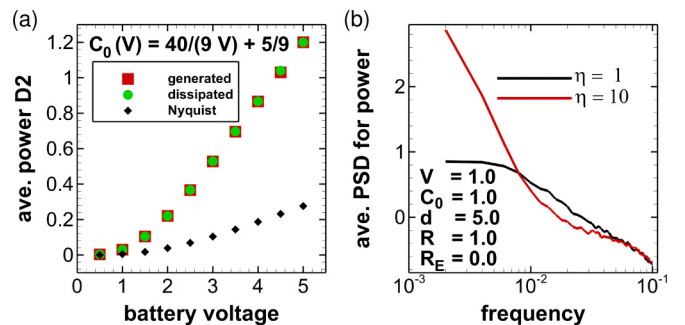

FIG. 6. Ito-Langevin equation simulation results for a circuit with diodes and resistor. (a) Average counterclockwise power versus battery voltage. (b) Average power spectrum density of power vs. frequency.

This increases the exact power above the Nyquist power, as shown in Fig. 6(a).

If we short circuit the diodes, then our thermal power formula might appear to be similar to the Nyquist result $\frac{V_{\mathcal{R}}^2}{\mathcal{R}} = \frac{T}{\mathcal{R}C}$, but this is purely formal. For Nyquist's result, the origin of the thermal noise is the resistor, and the role of the capacitor is to set the bandwidth. In contrast, for our model, the power includes contributions from the Brownian motion of the graphene ripple through a change in capacitance. As a result, the double-well potential introduces a new timescale, which is the barrier crossing rate. This gives rise to very low frequency oscillations, which were observed experimentally in an earlier study and which motivated this work [39]. To illustrate, the average power spectral density for the power dissipated at the resistor without diodes is plotted using two different velocity relaxation values for η of 1 and 10 in Fig. 6(b). The total power dissipated is the same, but increasing the relaxation time reduces the barrier crossing rate and therefore redistributes power to lower frequencies. This spectral redistribution of power adds technological value, as previously discussed by López-Suárez *et al.* [40]. Note that these results are shown for linear resistors, and the diodes are not responsible for this effect. It would be difficult to compare this prediction with the experiments, due to the STM instrumentation response. Nevertheless, we present this result to show that graphene is playing an essential role in the noise power, unlike a fixed capacitor. In addition, barrier crossing events are a proposed mechanism for producing $1/f$ noise, which this model quantitatively demonstrates [41].

C. Equilibrium average of the generated power

The overall equilibrium power due to the electric circuit is zero because the dissipated power at diodes and resistor are compensated exactly by the power generated by thermal fluctuations, which is the first term on the right-hand side of Eq. (12). In this section, we find approximate formulas for the equilibrium average of the generated power. This allows us to make a quantitative comparision of how the generated power varies with bias voltage. We show in Appendix B that the generated power is

$$\left\langle \frac{d'W}{dt} \right\rangle_g = \frac{\int e^{-\frac{\mathcal{H}}{T}} \frac{\partial}{\partial q}\left(\frac{\frac{\partial \mathcal{H}}{\partial q}}{R+R_E}\right) dx\, dp\, dq}{\int e^{-\frac{\mathcal{H}}{T}} dx\, dp\, dq}, \tag{13a}$$

$$= \frac{K(V)\int \sqrt{1+\frac{x}{d}}\, e^{-\frac{\mathcal{H}_r}{T}} dx}{\int \left(1+\frac{x}{d}\right)^{-1/2} e^{-\frac{\mathcal{H}_r}{T}} dx}, \tag{13b}$$

$$\mathcal{H}_r(x) = U(x) - \frac{C_0 V^2 \Gamma(V)}{2}\left(\frac{1}{1+\frac{x}{d}} + \frac{x}{d}\right), \tag{13c}$$

$$K(V) = \frac{2I_0 T}{\Gamma(V)C_0(T_e + 2I_0 R)}. \tag{13d}$$

The integrals in Eq. (13b), which are independent of the particle mass, can be evaluated approximately as follows.

The integration interval in Eq. (13b) is $[-d + \varepsilon d, \infty)$, where $\varepsilon d > 0$ is the minimum allowed distance between the graphene sample and the STM tip. This minimum distance is not known precisely from the experiment. However, we

will show that, when it is appreciable, the measured average dissipated power does not depend on the minimum distance. Thus, we do not need to know the latter. Clearly, the integrals in Eq. (13b) depend on the structure of the function $\mathcal{H}_r(x)$, which has a vertical asymptote at $x = -d$ and on ε.

1. Structure of $\mathcal{H}_r(x)$ for $x > -d$

First, we approximate the extrema of $\mathcal{H}_r(x)$ from

$$\frac{\partial \mathcal{H}_r}{\partial x} = x\left[\frac{U_B}{l^4}(x^2 - l^2) - \frac{C_0 V^2 \Gamma(V)}{2d^2}\frac{2+\frac{x}{d}}{\left(1+\frac{x}{d}\right)^2}\right]$$

$$= \frac{(X-1)d}{X^2 l^2}\left[\frac{U_B d^2}{l^2}\left(X^4 - 2X^3 + \frac{d^2 - l^2}{d^2}X^2\right)\right.$$

$$\left. - \frac{C_0 V^2 l^2 \Gamma(V)(X+1)}{2d^2}\right] = 0, \tag{14}$$

where $X = 1 + x/d$ and $d > l$. We see that $\mathcal{H}_r$ has a vertical asymptote at $X = 0$, an extremum at $x = 0$ (i.e., $X = 1$), one negative zero (only one change of sign between coefficients when $-X$ replaces X in this equation), and either one or three positive zeros X_0 of Eq. (14) (three changes of sign between coefficients).

Now both U_B/T and $C_0 V^2/T$ are large. Then, for a wide range of parameters, the following occurs: The positive solution near $X = 0$ comes from a balance between the two last terms in Eq. (14), i.e.,

$$X_0 \sim \frac{V l^2}{d}\sqrt{\frac{C_0 \Gamma(V)}{2U_B(d^2 - l^2)}} + \frac{C_0 V^2 \Gamma(V) l^4}{4U_B d^2(d^2 - l^2)}, \tag{15}$$

and $x_0 = (X_0 - 1)d < -l$ is a maximum of $\mathcal{H}_r$, as shown by calculating $\partial^2 \mathcal{H}_r/\partial x^2$ and using Eq. (14):

$$\frac{\partial^2 \mathcal{H}_r}{\partial x^2}(x_0) = \frac{x_0}{l^4}\left[2U_B x_0 + \frac{C_0 V^2 \Gamma(V) l^3}{2d^3}\frac{3+\frac{x_0}{d}}{\left(1+\frac{x_0}{d}\right)^3}\right]$$

$$= 2U_B \frac{x_0}{l^4}\left[\frac{x_0}{l} + \frac{(x_0^2 - l^2)(3d + x_0)}{2(x_0 + d)(2d + x_0)}\right] < 0. \tag{16}$$

Similarly, $x_0 = 0$ ($X_0 = 1$) is a maximum, which follows from Eq. (14). Then, for $V > 0$ and as x increases from $x = -d$ (where $\mathcal{H}_r$ as a vertical asymptote), $\mathcal{H}_r$ increases from $-\infty$ to a sharp maximum at X_0 approximately given by Eq. (15), decreases to a relatively shallow minimum near $x = -l$, increases to a maximum at $x_0 = 0$, decreases to a minimum near $x = l$, and then increases indefinitely. For example, for $V = 10$ V, the maximum of $H_r(x)/T$ is 4.5×10^{16} (reached just past the vertical asymptote at $x = -d$). The global minimum for $X > X_0$ given by Eq. (15) is -103.3 and is reached near $x = -l$. Thus, for $-d \leqslant x \leqslant d$, the lowest value of $\mathcal{H}_r$ is $-\infty$ at $x = -d$, whereas it is reached at the global minimum near $x = -d$ for $x > (-1 + X_0)d$.

2. Role of the minimum distance

The minimum allowed distance from graphene sheet to STM tip is $x_m + d = \varepsilon d$, i.e., $X_m = \varepsilon$. Then the average generated power is determined by the contribution to the integrals in Eq. (13b) at this minimum distance if $\varepsilon < X_0$, the maximum given by Eq. (15). If $\varepsilon > X_0$, then the integrals are dominated

by the contribution near the global minimum of $\mathcal{H}_r$. Since X_0 depends on V, its relative position with respect to ε may change with V.

We now calculate the average generated power using Eq. (13b) when the minimum distance satisfies $\varepsilon < X_0(V)$, given by Eq. (15):

$$\left\langle \frac{d'W}{dt} \right\rangle_g = K(V) \frac{\int_1^\infty \sqrt{y}\, e^{-\frac{\mathcal{H}_r(y)}{T}} dy}{\int_1^\infty y^{-1/2} e^{-\frac{\mathcal{H}_r(y)}{T}} dy}$$

$$= K(V) \frac{\left(\int_1^{X_0/\varepsilon} + \int_{X_0/\varepsilon}^\infty\right) \sqrt{y}\, e^{-\frac{\mathcal{H}_r(y)}{T}} dy}{\left(\int_1^{X_0/\varepsilon} + \int_{X_0/\varepsilon}^\infty\right) y^{-1/2} e^{-\frac{\mathcal{H}_r(y)}{T}} dy}. \quad (17)$$

Here we have changed variables as $x = (-1 + \varepsilon y)d$, i.e., $X = \varepsilon y$. The largest contribution to these integrals comes from the boundary terms $\int_1^{X_0/\varepsilon}$ in the numerator and denominator. Integration by parts yields the dominant contributions. Defining $a = C_0 V^2 \Gamma(V)/(2T)$, the integrals in numerator and denominator are as follows:

$$J_\pm(\varepsilon) = \int_1^{X_0/\varepsilon} y^{\pm 1/2} e^{a(\varepsilon y - 1) - U((\varepsilon y - 1)d)/T} e^{\frac{a}{\varepsilon y}} dy. \quad (18)$$

To approximate these integrals as $\varepsilon \to 0+$, we integrate by parts to get [42],

$$J_\pm(\varepsilon) = \frac{\varepsilon}{ae^a}\left(e^{\frac{a}{\varepsilon}} e^{-\frac{U[(\varepsilon-1)d]}{T}} - \left(\frac{X_0}{\varepsilon}\right)^{2\pm 1/2} e^{-\frac{U[(X_0-1)d]}{T}} e^{\frac{a}{X_0}} \right.$$

$$\left. + \int_1^{X_0/\varepsilon} e^{\frac{a}{(\varepsilon y)}} \frac{\partial}{\partial y} \left\{ y^{2\pm 1/2} e^{-\frac{U[(\varepsilon y - 1)d]}{T}} \right\} dy \right)$$

$$\sim \frac{\varepsilon e^{-a}}{a} e^{\frac{a}{\varepsilon}} e^{-\frac{U[(\varepsilon-1)d]}{T}}, \quad (19)$$

where the last result follows since the second term and the integral are much smaller. The other integrals in Eq. (17) are dominated by the contributions of the local positive minima that are the zeros of Eq. (14). However, in the limit $\varepsilon \to 0+$, these contributions are exponentially small with respect to that given by Eq. (19). We also have

$$\frac{J_+(\varepsilon)}{J_-(\varepsilon)} \sim 1 - \left(\frac{X_0}{\varepsilon} - 1\right)\left(\frac{X_0}{\varepsilon}\right)^{3/2} e^{\frac{a}{X_0}} e^{-\frac{a}{\varepsilon}}$$

$$\times e^{\frac{1}{T}\{U[(\varepsilon-1)d] - U[(X_0-1)d]\}} \sim 1, \quad (20)$$

as $\varepsilon \to 0+$. Thus, for $\varepsilon < X_0(V)$, the average generated power in Eq. (17) becomes

$$\left\langle \frac{d'W}{dt} \right\rangle_g \sim \varepsilon K(V) = \frac{2 I_0 T \varepsilon}{\Gamma(V) C_0 (T_e + 2 I_0 R)}. \quad (21)$$

Here $C_0 \Gamma(V)/\varepsilon = C_{\max}(V)$ is the maximum value of the capacitance, which is achieved at the cutoff minimum distance between graphene and STM tip. The average generated power of Eq. (21) tends to zero as $\varepsilon \to 0+$. We conclude that the average generated power is zero in equilibrium if the minimum distance cutoff is allowed to be zero. We have checked this conclusion by calculating numerically the cutoff integrals in Eq. (13b), confirming graphically that X_0 is a maximum of $\mathcal{H}_r$, and observing how the average generated power decreases as the cutoff decreases (up to 10^{-12}).

If $\varepsilon > X_0(V)$ (minimum cutoff distance larger than the sharp maximum near $-d$), then the integrals in Eq. (13b) can be approximated by the Laplace method [42] near the global minimum past the maximum at $X_0(V)$. Then the average generated power is

$$\left\langle \frac{d'W}{dt} \right\rangle_g \sim \frac{2 I_0 T}{\Gamma(V) C_0 (T_e + 2 I_0 R)}\left(1 + \frac{x_{0,m}}{d}\right)\left[1 - \frac{T l^2}{4 U_B (d-l)^2}\right]$$

$$\sim \frac{2 I_0 T}{\Gamma(V) C_0 (T_e + 2 I_0 R)}\left\{1 - \frac{l}{d} - \frac{C_0 V^2 \Gamma(V) l^3}{4 U_B d^2 (d-l)^2}\left[2d - l - \frac{4l^2 - 11 dl + 4 d^2}{4 U_B (d-l)^2} T l\right] - \frac{T l^2}{4 U_B d (d-l)}\right\}. \quad (22)$$

Here $x_{0,m}$ is the global minimum and the second approximate expression holds for small enough voltages V. Numerical calculations of the generated power in Eq. (13a) (with sufficiently large cutoff) show that Eq. (22) agrees quite well with it.

We point out that for our diode configuration, the average power generated in equilibrium through either diode is one half of those calculated before. For ideal diode characteristics and the moderate to large values of the current, each diode lets current pass in only one direction. Since both are supposed to be equal, their average generated powers are equal and they add to the overall power, which is twice that of the individual diodes.

V. COMPARING THEORY AND EXPERIMENTS

To make a quantitative comparison of the results of the theory with experiments, we use the following values of the parameters in the equations of motion (1)–(3): $U_B/4 = 1$ eV (bending energy of suspended graphene), $l = 1$ nm (ripple

height), $d = 10l$ (average distance between graphene and STM tip), $\eta/m = 1$ THz (acoustic phonon frequency) [1]. Using resistance and power data from the experimental measurements presented in Fig. 2, we estimate a capacitance near 1 fF for the tip-graphene junction, therefore $C_0 = 1$ fF. The particle mass corresponds to the mass of the atoms in the ripple below the STM tip, thereby $m = 2 \times 10^{-22} N_a$ kg, where we estimate $N_a = 10^4$. However, as noted before, the equilibrum averages are independent of m. Room temperature is $T = 25.7$ meV. In the equations for the circuit, the saturation current $I_0 = 1$ nA follows from data in Fig. 2. The series resistor R includes the series resistance of the diodes at high injection and the resistance of the circuit wires. We estimate $I_0 R = 0.09$ V, and then $I_0 T/(T_e + 2 I_0 R)/C_0 \approx 0.02$ pW. A reasonable fit to the measurements in Fig. 2(d) is the decreasing function

$$\Gamma(V) = \left\{1 + 170 \frac{\tanh\left[\frac{1}{980}\left(\frac{V}{V_0} - 9\right)^2\right]}{1 + e^{8(9 - \frac{V}{V_0})}}\right\}^{-1}, \quad (23)$$
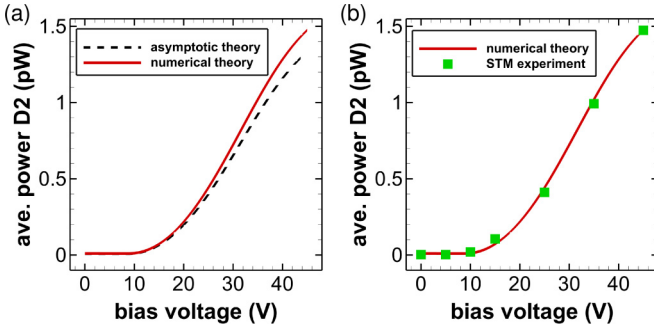
FIG. 7. Comparing numerical theory, approximate asymptotic theory, and STM experiments. (a) Numerically calculated (continuous red line), and approximate asymptotic (dotted line) equilibrium average of the power (in pW) dissipated at one diode versus the battery voltage (in volts). (b) Numerically calculated (continuous red line) and STM experimental data (green squares). The numerical theory refers to numerical evaluation of the integrals in Eq. (13b) using Mathematica and the asymptotic theory to Eq. (22). In both cases, $\Gamma(V)$ is given by Eq. (23).

where $V = 9V_0 = 9$ V is selected as the value at which the dissipated power in Fig. 2(d) appreciably departs from zero. The integrations over x in Eq. (13b) have a cutoff $\varepsilon > X_0$ for the voltage range up to 45 V considered in the experiments ($\varepsilon = l/d = 0.1$). We have used Mathematica to compute numerically the integrals appearing in Eq. (13b). Explaining why Eq. (23) is a good fit will surely require a more complex model than the Brownian particle of Eqs. (1).

While the equilibrium averages were reduced to 1D integrals that could be calculated numerically in a straightforward manner, the time averages require solving numerically the Ito-Langevin equations (3) and (4). The parameters involved in these equations (listed above) are too extreme and therefore the equations are too stiff for numerical integration out to the timescale of the STM experiments. Hence, we have integrated them (using the first-order Milstein algorithm [38]) with less extreme numerical parameter values and checked that time averages equal equilibrium averages for sufficiently large intervals of time. Thus, the agreement between fluctuating currents or average power obtained from experiments and from numerical simulations of the stochastic equations can only be qualitative. However, equilibrium averages are much less costly to calculate numerically. We also have accurate asymptotic approximations found in the previous section. Using them, we quantitatively fit the data of the dissipated power at diode 2 from experiments.

Equilibrium average of power dissipated at diode 2

The equilibrium average of the power dissipated at one diode is half the overall average dissipated power. As the equilibrium averages of dissipated and generated power are the same, the average dissipated power at one diode is one half of the power given by Eq. (13b). Figure 7(a) compares the result of direct numerical calculation of the equilibrium average of the dissipated power at one diode to one half the power given by Eq. (22). For the values extracted from our experimental configuration, there is good agreement between

the approximation of Eq. (22) and the direct numerical calculation of Eq. (13b). In both cases, $\Gamma(V)$ is given by Eq. (23). The agreement between the asymptotic and numerical results worsens as the voltage increases. However, Eq. (22) captures well the general trend of the average power dissipated at diode 2. The numerical theory fits well with the STM experimental result as shown in in Fig. 7(b).

VI. DISCUSSION AND SUMMARY

In this paper, we have studied theoretically and experimentally spontaneous thermal fluctuations of a graphene membrane coupled to a circuit with diodes having nonlinear current-voltage characteristics. We have developed a model in which fluctuating freestanding graphene and STM tip act as moving plates of a variable capacitor coupled to diodes and battery that supplies dc voltage. The graphene sheet appears as a soft membrane covered with ripples whose curvature fluctuates between concave and convex as it exchanges energy with the circuit and the thermal bath. We have modeled the atoms on the ripple opposed to the STM tip as a single mass particle in a double-well potential. The particle is subject to electrostatic forces opposed by the stretching reaction of other carbon atoms in the membrane, friction, and thermal noise. Electrostatic forces are induced by the variable distance between particle (i.e., the graphene ripple) and STM tip. In addition, the graphene capacitance decreases as the battery voltage increases. This effect mimics the increasing deformation of the membrane opposite the STM tip and causes the experimentally observed increment of the average dissipated power at the diodes. The nonlinear characteristics of the diodes require adding a temperature dependent drift to the stochastic Ito-Langevin equations of the circuit. These equations are different from those with the usual Nyquist noise of linear resistors and have not previously been studied using stochastic thermodynamics. The latter is necessary to consider the dynamics of fluctuations and to show that all energy dissipated at diodes and resistors is fully provided by the thermal bath, thus satisfying the second law of thermodynamics.

We have calculated the equilibrium average of power generated and dissipated at the diodes both numerically and by asymptotic approximations of integrals. Using realistic parameter values for graphene and others extracted from experiments, we see that these averages involve scales differing by many orders of magnitude. This means that the stochastic Ito-Langevin equations describing fluctuating dynamics are very stiff. Therefore, their numerical simulations are very costly and impractical. Thus, we have simulated these equations with milder numerical parameters. We have checked that long time averages of dissipated power at one diode are exactly the same as long time averages of power supplied by the thermal bath. Time averages agree with averages using the equilibrium probability density. The time averages of the positive and negative current are equal to each other. In turn, time averages of dissipated and generated powers of positive (respectively, negative) currents are also equal to each other.

In our experiments, we have studied the thermal fluctuations in freestanding graphene membranes using point-mode scanning tunneling microscopy. After disabling the STM feedback circuit, a displacement current was measured. We

measured the fluctuating current at the diodes, the fluctuating dissipated power, and its long time average. The latter is very small for values of battery voltage up to about 10 V. Then the average dissipated power increases noticeably. We used this observation to fit the graphene capacitance to an appropriate decreasing function of the bias voltage. We modeled the ripple closest to the STM tip as a Brownian particle in a double-well potential. When the graphene moves, charge must flow through the circuit and perform electrical work. Our model provides a rigorous demonstration that continuous thermal power can be supplied by a Brownian particle at a single temperature while in thermodynamic equilibrium, provided the *same amount* of power is continuously dissipated in a resistor. Here coupling to the circuit allows electrical work to be carried out on the load resistor without violating the second law of thermodynamics. Nonequilibrium fluctuations due to extra noises [43,44] or to different temperatures in electrical circuits [45] will produce entropy and measurable deviations from detailed balance [44,45] and are worth investigating in freestanding graphene.

APPENDIX A: MASTER EQUATION

Let us ignore the variation of x so that the graphene ripple and the STM tip behave as the fixed two plates of a capacitor. Following Landauer [46], van Kampen [47], and Sokolov [48,49], the probability of having n electrons in the STM tip satisfies the master equation

$$\dot{\rho}_n = w_{n+1,n}\rho_{n+1} + w_{n-1,n}p_{n-1}$$
$$- (w_{n,n+1} + w_{n,n-1})\,\rho_n. \tag{A1}$$

The transition probabilities per unit time, $w_{n,m}$, characterize the ways electrons can transfer between capacitor plates and also depend on the type of noise we consider. Here we consider thermal noise and ignore shot noise; see Ref. [46] for the latter. Then detailed balance implies [47,48]

$$\frac{w_{n,n+1}}{w_{n+1,n}} = \exp\left(-\frac{\mathcal{H}_{n+1} - \mathcal{H}_n}{T}\right) \equiv \exp\left(-\frac{D^+\mathcal{H}_n}{T}\right), \tag{A2}$$

where $\mathcal{H}_n$ is the Hamiltonian with n electrons and $D^+\mathcal{H}_n = \mathcal{H}_{n+1} - \mathcal{H}_n$ is a forward finite difference. Equations (A1) and (A2) imply

$$\dot{\rho}_n = D^+[w_{n,n-1}(\rho_n - e^{-D^+\mathcal{H}_{n-1}/T}\rho_{n-1})]. \tag{A3}$$

In the continuum limit $n \to \infty$ with fixed $q = ne$, a Taylor expansion of $\rho(ne, t) = \rho_n(t)$ and $w_{n,n-1} = w(ne)$ produces

the FPE

$$\frac{\partial\rho}{\partial t} = \frac{\partial}{\partial q}\left[\frac{e^2 w}{T}\left(\frac{\partial\mathcal{H}}{\partial q}\,\rho + T\frac{\partial\rho}{\partial q}\right)\right]. \tag{A4}$$

It remains to identify the quantity $e^2 w/T$. In the absence of noise, Kirchhoff's current law gives $\dot{q} = \dot{q}_1 + \dot{q}_2$, which together with Kirchhoff's voltage law

$$R\dot{q} + V + \frac{q}{C} - u = 0, \quad \dot{q}_j = -\frac{u}{R_j}, \tag{A5}$$

yield

$$u = \frac{V + \frac{q}{C}}{1 + \frac{R}{R_1} + \frac{R}{R_2}} = \frac{1}{1 + \frac{R}{R_E}}\left(V + \frac{q}{C}\right). \tag{A6}$$

Since $R_E^{-1}(u) = 2I_0 \sinh(u/T_e)/u$, this expression yields the following relation between the potential drop at the diodes, u, and the overall charge q:

$$u + 2I_0 R \sinh\left(\frac{u}{T_e}\right) = V + \frac{q}{C}. \tag{A7}$$

Substituting Eq. (A6) into the Kirchhoff voltage law, we obtain the following deterministic equation for q:

$$\dot{q} = -\frac{1}{R + R_E}\left(V + \frac{q}{C}\right), \tag{A8}$$

which coincides with Eq. (5) if $T = 0$ and we keep only the circuit part of the model. Ignoring diffusion, the drift part of the FPE (A4) has characteristic curves

$$\frac{dq}{dt} = -\frac{e^2 w}{T}\frac{\partial\mathcal{H}}{\partial q} = -\frac{e^2 w}{T}\left(V + \frac{q}{C}\right).$$

This expression agrees with Eq. (A8) provided we identify

$$\frac{e^2 w}{T} = \frac{1}{R + R_E} = \frac{1}{\mathcal{R}}. \tag{A9}$$

Then the FPE (A4) becomes

$$\frac{\partial\rho}{\partial t} = \frac{\partial}{\partial q}\left[\frac{1}{\mathcal{R}}\left(\frac{\partial\mathcal{H}}{\partial q}\,\rho + T\frac{\partial\rho}{\partial q}\right)\right]$$
$$= \frac{\partial}{\partial q}\left[\frac{\rho}{\mathcal{R}}\frac{\partial\mathcal{H}}{\partial q} - \rho\frac{\partial}{\partial q}\left(\frac{T}{\mathcal{R}}\right) + \frac{\partial}{\partial q}\left(\frac{T\rho}{\mathcal{R}}\right)\right]. \tag{A10}$$

Adding the terms corresponding to the Brownian particle, we complete the FPE (5).

APPENDIX B: EQUILIBRIUM AVERAGE OF THE GENERATED POWER

To derive Eq. (13b), we need to reduce the triple integrals in Eq. (13a) to single integrals. To this end, we have used Eqs. (4b) and (6) and the following formula that comes from differentiation of Eq. (6):

$$\frac{\partial u}{\partial q} = \frac{1}{C(x)\left[1 + \frac{2I_0 R}{T_e}\cosh\left(\frac{u}{T_e}\right)\right]}. \tag{B1}$$

First, we obtain

$$\frac{\partial}{\partial q}\left(\frac{T}{R+R_E}\frac{\partial\mathcal{H}}{\partial q}\right) = 2TI_0\frac{\partial}{\partial q}\left[\sinh\left(\frac{u}{T_e}\right)\right]$$

$$= \frac{2I_0 T}{T_e}\cosh\left(\frac{u}{T_e}\right)\frac{\partial u}{\partial q}$$

$$= \frac{2eI_0\cosh\left(\frac{u}{T_e}\right)}{C(x)\left[1+\frac{2I_0 R}{T_e}\cosh\left(\frac{u}{T_e}\right)\right]}. \quad \text{(B2)}$$

Second, we calculate the Gaussian integrals over q in Eq. (13a). To this end, we note that

$$\int f(q)\, e^{-\frac{\mathcal{H}}{T}}\, dq = f\left(-T\frac{\partial}{\partial\zeta}\right)\int e^{-\frac{\tilde{\mathcal{H}}}{T}}\, dq\bigg|_{\zeta=0}, \quad \text{(B3)}$$

$$\tilde{\mathcal{H}}(x,p,q,\zeta) = \mathcal{H}(x,p,q) + q\zeta. \quad \text{(B4)}$$

The energy $\tilde{\mathcal{H}}(x,p,q,\zeta)$ can be written as

$$\tilde{\mathcal{H}}(x,p,q,\zeta) = \frac{p^2}{2m} + U(x) - \frac{C_0 V^2 x}{2d} + \frac{[q+C(x)(V+\zeta)]^2}{2C(x)}$$

$$- \frac{1}{2}C(x)(V+\zeta)^2. \quad \text{(B5)}$$

The Gaussian integrals over p and q can be performed by completing squares with the result

$$\int e^{-\frac{\tilde{\mathcal{H}}}{T}}\, dp\, dq = 2\pi T\sqrt{mC(x)}\, e^{-\frac{\tilde{\mathcal{H}}_r}{T}}, \quad \text{(B6)}$$

$$\tilde{\mathcal{H}}_r(x,\zeta) = U(x) - \frac{C_0 V^2 x}{2d} - \frac{1}{2}C(x)(V+\zeta)^2. \quad \text{(B7)}$$

Then the derivative with respect to ζ that appears in Eq. (B3) produces an argument $q = -C(x)V$ for $\zeta = 0$. Inserting this in Eq. (A7), we obtain the solution $u = 0$. For $u = 0$, Eq. (B2) becomes

$$\frac{\partial}{\partial q}\left(\frac{T}{R+R_E}\frac{\partial\mathcal{H}}{\partial q}\right) = \frac{2TI_0\left(1+\frac{x}{d}\right)}{C_0\Gamma(V)(T_e+2I_0 R)}. \quad \text{(B8)}$$

Using Eq. (B6) and (B8), we find

$$\left\langle\frac{d'W}{dt}\right\rangle_g = \frac{2TI_0\int\left(1+\frac{x}{d}\right)^{\frac{1}{2}}e^{-\frac{\mathcal{H}_r}{T}}dx}{C_0\Gamma(V)(T_e+2I_0 R)\int\left(1+\frac{x}{d}\right)^{-\frac{1}{2}}e^{-\frac{\mathcal{H}_r}{T}}dx}, \quad \text{(B9)}$$

which is Eq. (13b). Here $\mathcal{H}_r(x) = \tilde{\mathcal{H}}_r(x,0)$ is the same as in Eq. (13c).

[1] A. H. Castro Neto, F. Guinea, N. M. R. Peres, K. S. Novoselov, and A. K. Geim, The electronic properties of graphene, Rev. Mod. Phys. **81**, 109 (2009).

[2] M. L. Ackerman, P. Kumar, M. Neek-Amal, P. M. Thibado, F. M. Peeters, and S. Singh, Anomalous Dynamical Behavior of Freestanding Graphene Membranes, Phys. Rev. Lett. **117**, 126801 (2016).

[3] J. C. Meyer, A. K. Geim, M. I. Katsnelson, K. S. Novoselov, T. J. Booth, and S. Roth, The structure of suspended graphene sheets, Nature **446**, 60 (2007).

[4] A. Fasolino, J. H. Los, and M. I. Katsnelson, Intrinsic ripples in graphene, Nat. Mater. **6**, 858 (2007).

[5] N. Abedpour, M. Neek-Amal, R. Asgari, F. Shahbazi, N. Nafari, and M. R. Tabar, Roughness of undoped graphene and its short-range induced gauge field, Phys. Rev. B **76**, 195407 (2007).

[6] D. Gazit, Correlation between charge inhomogeneities and structure in graphene and other electronic crystalline membranes, Phys. Rev. B **80**, 161406(R) (2009).

[7] P. San-José, J. González, and F. Guinea, Electron-Induced Rippling in Graphene, Phys. Rev. Lett. **106**, 045502 (2011).

[8] F. Guinea, P. Le Doussal, and K. J. Wiese, Collective excitations in a large-d model for graphene, Phys. Rev. B **89**, 125428 (2014).

[9] L. L. Bonilla and M. Ruiz-Garcia, Critical radius and temperature for buckling in graphene, Phys. Rev. B **93**, 115407 (2016).

[10] T. Cea, M. Ruiz-García, L. L. Bonilla, and F. Guinea, A numerical study of rippling instability driven by the electron-phonon coupling in finite size graphene membranes, Phys. Rev. B **101**, 235428 (2020).

[11] L. L. Bonilla, A. Carpio, A. Prados, and R. R. Rosales, Ripples in a string coupled to Glauber spins, Phys. Rev. E **85**, 031125 (2012).

[12] L. L. Bonilla and A. Carpio, Ripples in a graphene membrane coupled to Glauber spins, J. Stat. Mech. (2012) P09015.

[13] M. Ruiz-Garcia, L. L. Bonilla, and A. Prados, Ripples in hexagonal lattices of atoms coupled to Glauber spins, J. Stat. Mech. (2015) P05015.

[14] R. Zan, U. Bangert, C. Muryn, P. Mattocks, B. Hamilton, and K. S. Novoselov, Scanning tunneling microscopy of suspended graphene, J. Phys.: Conf. Ser. **371**, 012070 (2012).

[15] R. Zan, C. Muryn, U. Bangert, P. Mattocks, P. Wincott, D. Vaughan, X. Li, L. Colombo, R. S. Ruoff, B. Hamilton, and K. S. Novoselov, Scanning tunneling microscopy of suspended graphene, Nanoscale **4**, 3065 (2012).

[16] N. N. Klimov, S. Jung, S. Zhu, T. Li, C. A. Wright, S. D. Solares, D. B. Newell, N. B. Zhitenev, and J. A. Stroscio, Electromehcnical properties of graphene drumheads, Science **336**, 1557 (2012).

[17] P. Xu, Y. Yang, S. D. Barber, M. L. Ackerman, J. K. Schoelz, D. Qi, I. A. Kornev, L. Dong, L. Bellaiche, S. Barraza-Lopez, and P. M. Thibado, Atomic control of strain in freestanding graphene, Phys. Rev. B **85**, 121406(R) (2012).

[18] X. Zhao, X. Zhai, A. Zhao, B. Wang, and J. G. Hou, Fabrication and scanning tunneling microscopy charaterization of suspended monolayer graphene on periodic Si nanopillars, Appl. Phys. Lett. **102**, 201602 (2013).

[19] Z. Osvath, F. Lefloch, V. Bouchiat, and C. Chapelier, Electric field-controlled rippling of graphene, Nanoscale **5**, 10996 (2013).

[20] R. Breitwieser, Y. C. Hu, Y. C. Chao, R. J. Li, Y. R. Tzeng, L. J. Li, S. C. Liou, K. C. Lin, C. W. Chen, and W. W. Pai, Flippling nanoscale ripples of free-standing graphene using a scanning tunneling microscope tip, Carbon **77**, 236 (2014).

[21] J. K. Schoelz, P. Xu, V. Meunier, P. Kumar, M. Neek-Amal, P. M. Thibado, and F. M. Peeters, Graphene ripples as a realization of a two-dimensional Ising model: A scanning tunneling microscope study, Phys. Rev. B **91**, 045413 (2015).

[22] B. Uder and U. Hartmann, A convenient method for large-scale STM mapping of freestanding atomically thing conductive membranes, Rev. Sci. Instrum. **88**, 063702 (2017).

[23] R. Breitwieser, Y. C. Hu, Y. C. Chao, Y. R. Tzeng, S. C. Liou, K. C. Lin, C. W. Chen, and W. W. Pai, Investigating ultraflexible freestanding graphene by scanning tunneling microscopy and spectroscopy, Phys. Rev. B **96**, 085433 (2017).

[24] B. Uder, H. Gao, P. Kunnas, N. de Jonge, and U. Hartmann, Low-force spectroscopy on grpahene membranes by scanning tunneling microscopy, Nanoscale **10**, 2148 (2018).

[25] E. V. Castro, H. Ochoa, M. I. Katsnelson, R. V. Gorbachev, D. E. Elias, K. S. Novoselov, A. K. Geim, and F. Guinea, Limits on Charge Carrier Mobility in Suspended Graphene Due to Flexural Phonons, Phys. Rev. Lett. **105**, 266601 (2010).

[26] K. Sekimoto, *Stochastic Energetics* (Springer, New York, 2010).

[27] N. G. Van Kampen, *Stochastic Processes in Physics and Chemistry* (Elsevier, Amsterdam 2003).

[28] M. Ruiz-Garcia, L. L. Bonilla, and A. Prados, STM-driven transition from rippled to buckled graphene in a spin-membrane model, Phys. Rev. B **94**, 205404 (2016).

[29] J. S. Bunch, S. S. Verbridge, J. S. Alden, A. M. van der Zande, J. M. Parpia, H. G. Craighead, and P. L. McEuen, Impermeable atomic membranes from graphene sheets, Nano Lett. **8**, 2458 (2008).

[30] J. F. Xu, P. M. Thibado, and Z. Ding, 4 K, ultrahigh vacuum scanning tunneling microscope having two orthogonal tips with tunnel junctions as close as a few nanometers, Rev. Sci. Instrum. **77**, 093703 (2006).

[31] M. AbdelGhany, F. Mahvash, M. Mukhopadhyay, A. Favron, R. Martel, M. Siaj, and T. Szkopek, Suspended graphene variable capacitor, 2D Mater. **3**, 041005 (2016).

[32] S. F. Philp, The vacuum-insulated, varying capacitance machine, IEEE Trans. Electr. Insul. **EI-12**, 130 (1977).

[33] N. R. Greene, Energy flow for a variable-gap capacitor, Phys. Teach. **43**, 340 (2005).

[34] R. O'Donnell, N. Schofield, A. C. Smith, and J. Cullen, Design concepts for high-voltage variable-capacitance DC generators, IEEE Trans. Ind. Appl. **45**, 1778 (2009).

[35] P. Xu, S. D. Barber, M. L. Ackerman, J. K. Schoelz, and P. M. Thibado, Role of bias voltage and tunneling current in the perpendicular displacements of freestanding graphene via scanning tunneling microscopy, J. Vac. Sci. Technol. B **31**, 04D103 (2013).

[36] H. Nyquist, Thermal agitation of electric charge in conductors, Phys. Rev. **32**, 110 (1928).

[37] H. Risken, *The Fokker-Planck Equation*, 2nd ed. (Springer, Berlin, 1989).

[38] C. W. Gardiner, *Stochastic Methods: A Handbook for the Natural and Social Sciences* 4th ed. (Springer, Berlin, 2010).

[39] P. Xu, M. Neek-Amal, S. D. Barber, J. K. Schoelz, M. L. Ackerman, P. M. Thibado, A. Sadeghi, and F. M. Peeters, Unusual ultra-low-frequency fluctuations in freestanding graphene, Nat. Commun. **5**, 3720 (2014).

[40] M. López-Suárez, R. Rurali, L. Gammaitoni, and G. Abadal, Nanostructured graphene for energy harvesting, Phys. Rev. B **84**, 161401(R) (2011).

[41] P. Dutta and P. M. Horn, Low-frequency fluctuations in solids: $1/f$ noise, Rev. Mod. Phys. **53**, 497 (1981).

[42] C. M. Bender and S. A. Orszag, *Advanced Mathematical Methods for Scientists and Engineers* (McGraw–Hill, New York, 1978).

[43] C. R. Doering, W. Horsthemke, and J. Riordan, Nonequilibrium Fluctuation-Induced Transport, Phys. Rev. Lett. **72**, 2984 (1994).

[44] A. Ghanta, J. C. Neu, and S. W. Teitsworth, Fluctuation loops in noise-driven linear dynamical systems, Phys. Rev. E **95**, 032128 (2017).

[45] J. P. Gonzalez, J. C. Neu, and S. W. Teitsworth, Experimental metrics for detection of detailed balance violation, Phys. Rev. E **99**, 022143 (2019).

[46] R. Landauer, Fluctuations in bistable tunnel diode circuits, J. Appl. Phys. **33**, 2209 (1962).

[47] N. G. van Kampen, Non-linear thermal fluctuations in a diode, Physica **26**, 585 (1960).

[48] I. M. Sokolov, On the energetics of a nonlinear system rectifying thermal fluctuations, EPL **44**, 278 (1998).

[49] I. M. Sokolov, Reversible fluctuation rectifier, Phys. Rev. E **60**, 4946 (1999).